

Cognition to Control – Multi-Agent Learning for Human-Humanoid Collaborative Transport

Hao Zhang^{1,2}, Ding Zhao² and H. Eric Tseng¹

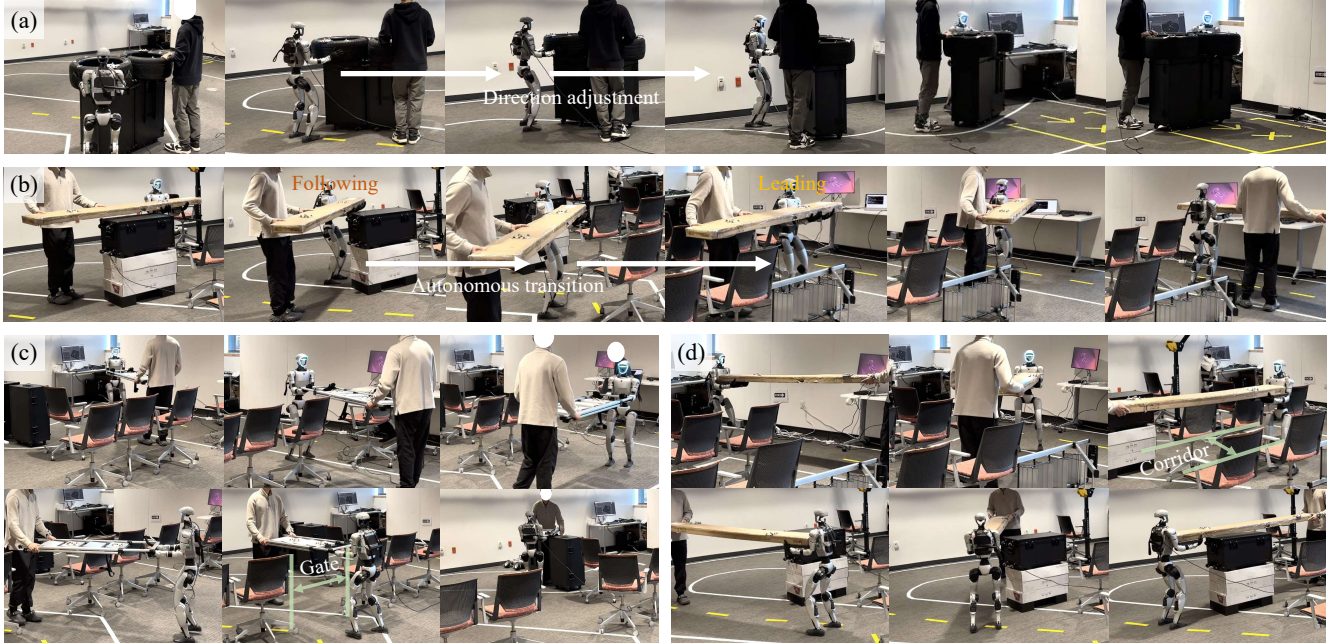


Fig. 1: Demonstration of human-robot collaboration via cognition-to-control hierarchy: (a) the humanoid and human partner collaboratively transport a caster-mounted object while performing real-time heading adjustments; (b) seamless transition between the following and leading roles during the cooperative task; (c) coordination between the humanoid and human to pass through a constrained gate; (d) stable super-long object transport throughout a corridor.

Abstract—Effective human-robot collaboration (HRC) requires translating high-level intent into contact-stable whole-body motion while continuously adapting to a human partner. Many vision-language-action (VLA) systems learn end-to-end mappings from observations and instructions to actions, but they often emphasize reactive (System 1-like) behavior and leave under-specified how sustained System 2-style deliberation can be integrated with reliable, low-latency continuous control. This gap is acute in multi-agent HRC, where long-horizon coordination decisions and physical execution must co-evolve under contact, feasibility, and safety constraints. We address this limitation with cognition-to-control (C2C), a three-layer hierarchy that makes the deliberation-to-control pathway explicit: (i) a VLM-based grounding layer that maintains persistent scene referents and infers embodiment-aware affordances/constraints; (ii) a deliberative skill/coordination layer—the System 2 core—that optimizes long-horizon skill choices and sequences under human-robot

coupling via decentralized MARL cast as a Markov potential game with a shared potential encoding task progress; and (iii) a whole-body control layer that executes the selected skills at high frequency while enforcing kinematic/dynamic feasibility and contact stability. The deliberative layer is realized as a residual policy relative to a nominal controller, internalizing partner dynamics without explicit role assignment. Experiments on collaborative manipulation tasks show higher success and robustness than single-agent and end-to-end baselines, with stable coordination and emergent leader-follower behaviors.

I. INTRODUCTION

Human-robot physical collaboration (HRC) is a foundational capability for the next generation of assistive and industrial robotics, where agents must maintain stable physical coupling while executing complex, long-horizon transport tasks [1]. Unlike traditional autonomous navigation, HRC is characterized by continuous bilateral interaction, where the system's state is simultaneously driven by the robot's control law and the inherent behavioral variability of a human partner [2]. This intrinsic coupling necessitates a high degree of mutual adaptation, as any misalignment in movement or intent can manifest as detrimental interaction, jeopardizing

*This work was supported by the University of Texas at Arlington and Carnegie Mellon University. Correspondance to H. Eric Tseng (hongtei.tseng@uta.edu) and Ding Zhao (dingzhao@cmu.edu).

¹Hao Zhang and H. Eric Tseng are with Department of Electrical Engineering, the University of Texas at Arlington, 76010 Arlington, USA haoz4@andrew.cmu.edu; hongtei.tseng@uta.edu

²Hao Zhang and Ding Zhao are with Department of Mechanical Engineering, Carnegie Mellon University, 15213 Pittsburgh, USA haoz4@andrew.cmu.edu; dingzhao@cmu.edu

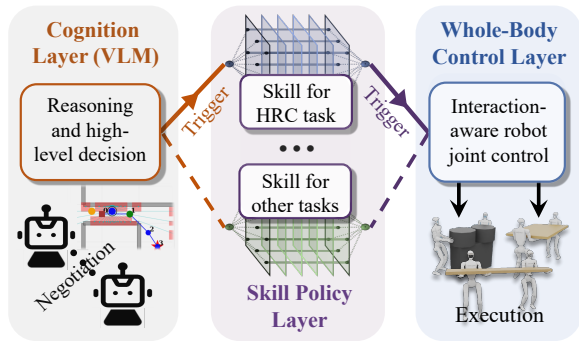


Fig. 2: Overview of the proposed cognitive-to-physical hierarchy for HRC decision partitioned into decoupled layers.

both working efficiency and human safety [3].

To manage these interaction dynamics, early research has predominantly relied on explicit role assignment (leader-follower), intent inference, or hand-designed coordination scripts [4]. While these frameworks provide a degree of stability in controlled settings, they are limited by their reliance on pre-defined heuristics. Such reactive systems often struggle to generalize when human behavior deviates from modeled assumptions, leading to brittle performance in unstructured environments where the partner’s strategy is neither constant nor predictable [5]. Consequently, the rigid nature of scripted coordination remains a primary bottleneck for deploying humanoids in human-populated scenarios. Recent literature has sought to overcome these limitations by employing reinforcement learning (RL) to model the partner as part of a stochastic environment or by augmenting policies with latent intent [6], [7]. However, treating the human as a passive environmental component fails to utilize the exploration opportunity during co-evolving. Furthermore, the introduction of explicit intent-inference modules often creates artificial non-stationarity during the optimization process [8]. As the robot adapts to human, the human concurrently adjusts to the robot, leading to oscillatory behaviors or catastrophic failures in contact-rich tasks [9]. This underscores a critical need for a learning paradigm that can internalize mutual adaptation as an intrinsic property rather than an external estimation [10].

Beyond the challenges of physical coordination, a significant cognitive-to-physical gap persists in existing HRC pipelines [11]. Although high-level quasi-static reasoning—such as navigating through a cluttered corridor to the destination—requires long-horizon cognitive planning ability, low-level physical stabilization demands reactive high-frequency control [12]. Conventional systems typically bridge this gap using occupancy-grid-based pathfinders, which lack the flexibility to incorporate open-vocabulary semantic cues or handle the resolution-frequency trade-offs inherent in multi-agent transport [13]. Recent advancements in vision-language models (VLMs) offer a promising alternative for adaptive reasoning [14], yet grounding such inner monologues into robust physical execution remains non-trivial [15]. The inability to seamlessly ground strategic intent into tactical

maneuvers remains a major obstacle in achieving fluid, human-like collaboration [16]. In summary, despite significant progress, existing HRC frameworks continue to suffer from the brittleness of heuristic scripts, the non-stationarity of single-agent learning abstractions, and the disconnect between semantic reasoning and physical grounding. To the best of the authors’ knowledge, a unified architecture that can simultaneously resolve open-vocabulary strategic goals while facilitating emergent, role-free tactical coordination remains a critical research gap.

To address these challenges, we propose cognition-to-control (C2C), a three-layer hierarchy that makes the deliberation-to-control pathway explicit for human–robot collaboration, decomposing HRC into semantic cognition, tactical skill, and physical execution layers. Our framework utilizes VLMs for strategic spatial grounding and MARL for tactical adaptation. By formulating HRC as an object-centric Markov potential game, we enable stable coordination and role transitions to emerge naturally from the task manifold, supported by a high-frequency whole-body control (WBC) kernel. The primary contributions are: 1) a hierarchical HRC architecture that decouples semantic reasoning from tactical physical coordination, effectively bridging the gap between high-level navigation and high-frequency execution; 2) a unified MARL-based formulation of HRC as a task-centric Markov potential game, which eliminates the need for explicit role assignment or intent inference and enables emergent, role-free mutual adaptation; 3) the proposed method is validated through spatially-confined heavy-duty cooperative transport experiments, demonstrating superior resilience to diverse tasks and human maneuvers with environmental constraints.

II. RELATED WORK

A. VLM-based Planning and Granularity Bottlenecks

Integrating VLMs and vision-language-action (VLA) models has advanced robotic reasoning and open-vocabulary decomposition [17], [18]. However, a granularity gap persists in physical HRC [19]: current VLAs typically output low-frequency discrete tokens, suitable for long-horizon tasks like SayCan [20] but inadequate for the high-frequency, continuous kinodynamic synchronization required in heavy-duty transport. While VLMs excel at strategic “where to go” reasoning, they lack the reactive bandwidth for millisecond-level force coupling. We bridge this by restricting the VLM to coarse strategic anchoring, delegating fine-grained tactical coordination to a high-frequency MARL layer.

B. Scripted and Single-Agent Approaches to HRC

Traditional HRC relies on impedance control or hand-crafted state machines to manage interaction via spring-damper dynamics [21]. Though safe, these methods scale poorly to complex, unstructured environments. Recent learning-based paradigms employ single-agent RL (SARL) with human motion predictors [2], yet they often treat the human as a passive environmental disturbance. This asymmetric modeling ignores the reciprocal adaptation inherent in

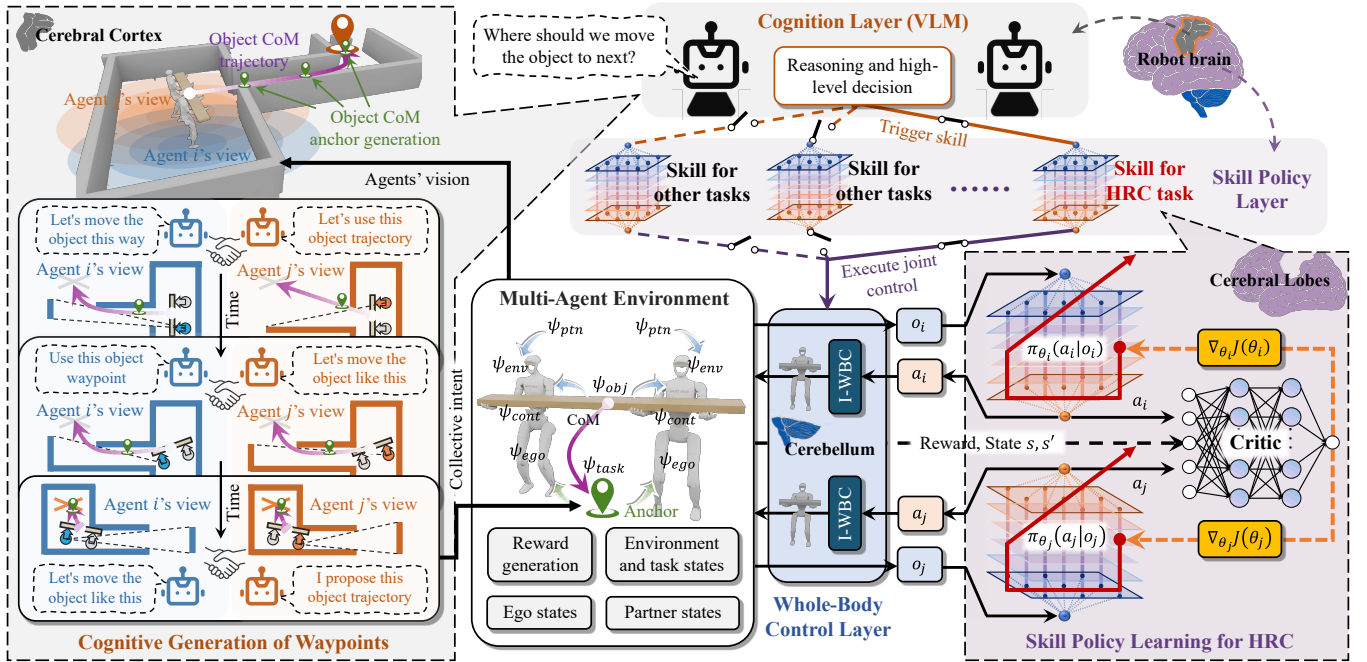


Fig. 3: The proposed hierarchical HRC framework for humanoid-object coordination, partitioning decision-making into three cascade layers: a cognition layer (VLM) generates semantic-aware object moving direction (anchors) from visual input; a skill policy layer (MARL), where agents maintain independent, to derive tactical coordination commands; and a cerebellum layer (WBC) for high-frequency whole-body stabilization and joint-level execution.

HRC, leading to brittle performance when human strategies deviate from the robot’s fixed assumptions [22].

C. Role-Based and Intent-Aware Collaboration Models

To handle behavioral variability, many frameworks utilize explicit leader-follower roles or intent-prediction mechanisms [23]. While these attempt to stabilize interaction by adjusting robot compliance, they introduce significant non-stationarity and prediction errors into the optimization loop. As the robot updates its belief of human intent, the human concurrently adapts their strategy, creating a shifting optimization target that causes oscillatory behaviors and limits generalization beyond training distributions [24].

D. Joint Evolution of Multi-Agent Reinforcement Learning

MARL has shifted coordination from centralized planning toward emergent decentralized behaviors [25]. Unlike expert-led systems, MARL in cooperative settings enables mutual adaptation through concurrent tabula rasa learning [26], [27]. This process forces agents to navigate diverse interactive configurations, serving as a natural data augmentation mechanism that densifies the experienced interaction space. By recovering from divergent patterns during training, the policy develops inherent resilience to unconventional partner behaviors, significantly mitigating out-of-distribution (OOD) risks during real-world deployment [28].

III. METHODOLOGY

The proposed framework addresses the intrinsic complexity of human–robot physical collaboration by partitioning the

decision process into three functionally decoupled layers: a collaborative cognitive layer, a skill policy layer, and a low-level execution layer. This hierarchy enables the system to bridge the gap between multi-view reasoning and high-frequency body execution, as illustrated in Fig. 3.

A. Hierarchical Task-Centric MARL Formulation

We formulate the collaborative transport task as a task-centric Markov potential game. While traditional multi-agent coordination can exhibit oscillatory best-response behavior, our task-centric formulation induces a shared potential function that aligns incentives; under standard better-/best-response (or potential-ascent) dynamics, this converges to a local equilibrium. The decision flow \mathcal{F} is structured as a hierarchical composition:

$$\mathcal{F} = \mathcal{F}_{WBC} \circ \mathcal{F}_{MARL} \circ \mathcal{F}_{COG} \quad (1)$$

1) *Collaborative cognitive layer* (\mathcal{F}_{COG}): Functioning as the cerebral cortex, this layer leverages decentralized VLM-based cognitive engines. For each agent i , the cognitive layer infers a shared task specification $\mathcal{T} = \{w_k\}_{k=1}^K$ from egocentric observations. In general, \mathcal{T} can be viewed abstractly as a task manifold (i.e., a constraint set or trajectory subset in task space). In this work, however, \mathcal{T} is instantiated concretely as a planar anchor (waypoint) sequence $\{w_k\} \subset \mathbb{R}^2$ that defines a shared reference path for the object CoM.

2) *Skill policy layer* (\mathcal{F}_{MARL}): Acting as the cerebral lobes, this layer optimizes decentralized skill policies $\pi_i(a_i|o_i, \mathcal{T})$. To ensure coordinated ascent, we define the reward R_i such

that the game satisfies the potential condition:

$$R_i(s, a'_i, a_{-i}) - R_i(s, a_i, a_{-i}) = \Phi(s, a'_i, a_{-i}) - \Phi(s, a_i, a_{-i}) \quad (2)$$

where the potential function Φ represents the negative distance to the manifold \mathcal{T} . In practice, we use a shared team reward, i.e., $R_i \equiv R_t$ for all agents, which is an identical-interest special case of a Markov potential game with potential $\Phi \equiv R_t$ (up to shaping). This formulation transforms the multi-agent conflict into a collaborative optimization of the residual coordination commands $\mathbf{u}_{i,t}$, facilitating emergent mutual adaptation without centralized gradients.

3) *Whole-body control layer* (\mathcal{F}_{WBC}): Analogous to cerebellum, a high-rate execution controller operating at f_{high} . It maps the MARL outputs $\mathbf{u}_{i,t}$ —residual task-space coordination commands—into joint-level torques $\boldsymbol{\tau}$ while enforcing contact stability and kinematic/dynamic feasibility.

B. Cognitive Layer: Decentralized Multi-View Consensus

The cognitive grounding layer \mathcal{F}_{COG} fuses multiple egocentric views into a shared task specification for downstream coordination and control. It outputs (i) a consensus anchor sequence \mathcal{T} and (ii) a task-guidance vector ψ_{task} for the skill-policy layer. This formulation ensures that decentralized tactical solvers are grounded in a globally consistent strategic agreement, transforming the HRC task from independent reactions into an execution of a shared cognitive plan:

1) *Spatial grounding via distributed perspectives*: To bridge continuous scene geometry with language-driven task intent, each agent i constructs an egocentric 2D overhead representation $\mathcal{I}_{env,i}$ from local geometric observations. We discretize $\mathcal{I}_{env,i}$ with an $M \times M$ grid \mathcal{P} and propose candidate waypoints for the object’s center of mass (CoM) under local obstacles and visibility constraints. From the grounded map, each agent also infers embodiment-specific feasibility constraints (e.g., collision-free corridors, clearance limits, and contact/approach constraints), and filters candidate anchors to those executable under the agent’s kinematics.

2) *Visual prompting and collective intent synthesis*: Each agent queries a local VLM module to propose task-relevant next anchors from its egocentric view. Agents then exchange compact summaries of these proposals and reconcile them into a globally consistent collective intent Ψ_{obj} , yielding a consensus anchor sequence $\mathcal{T} = \{\mathbf{w}_k\}_{k=1}^K$. The resulting anchors are provided to the MARL layer as task guidance; the skill-policy layer constructs the feature ψ_{task} from \mathcal{T} and the current object state as defined in Section III-C.

C. Skill Policy Layer: Tactical Coordination via MARL

The skill policy layer \mathcal{F}_{MARL} maps VLM-consensus anchors to coordination commands. To accommodate heterogeneous human–robot embodiments, agents maintain independent policies without parameter sharing, i.e., $\{\pi_{\theta_i}\}_{i \in \mathcal{N}}$. Embodiment awareness enters through (i) agent-specific policies and observations (ψ_{ego}, ψ_{ptn}) and (ii) residual task-space commands that are realized through each agent’s own kinematics.

1) *Observation space construction*: We define an observation $o_{i,t} \in \mathbb{R}^{\dim}$ to ensure decision-making sufficiency under partial observability:

$$o_{i,t} = [\psi_{task}, \psi_{ego}, \psi_{ptn}, \psi_{obj}, \psi_{cont}, \psi_{env}]. \quad (3)$$

Strategic guidance (ψ_{task}): To track the VLM anchor sequence $\mathcal{T} = \{\mathbf{w}_k\}_{k=1}^K$, we take a sliding window of length L and express anchors relative to the current object planar position $\mathbf{p}_{obj,t} \in \mathbb{R}^2$:

$$\psi_{task} = \{\mathbf{w}_k - \mathbf{p}_{obj,t}\}_{k=i}^{i+L-1} \in \mathbb{R}^{2L}, \quad (4)$$

where $\mathbf{w}_k \in \mathbb{R}^2$ are anchors in the same planar frame.¹

Kinematic and interaction states: Features ψ_{ego} and ψ_{ptn} capture proprioceptive and partner states (e.g., velocities \mathbf{v} , yaw ϕ , CoM height H , and relative end-effector positions \mathbf{p}_{ee}). Object geometry ψ_{obj} encodes the object state (pose \mathbf{x}_{obj} , velocity $\dot{\mathbf{x}}_{obj}$, and corner coordinates \mathcal{C}_{obj}), while the binary vector ψ_{cont} provides contact feedback.

Temporal context and environment: To capture interaction gradients without recurrent overhead, we stack three consecutive frames $\tilde{o}_{i,t} = [o_{i,t}, o_{i,t-1}, o_{i,t-2}]$. Obstacle awareness is provided by a LiDAR-like synthetic rangefinder $\psi_{env} \in \mathbb{R}^{n_{ray}}$, where n_{ray} is the number of rays and each detection d_j is normalized as:

$$\psi_{env,j} = 1 - \min(d_j, d_{max})/d_{max}. \quad (5)$$

2) *Residual action parameterization*: The policy π_{θ_i} outputs a continuous action $\mathbf{a}_{i,t} \in [-1, 1]^{11}$. To decouple tactical coordination from nominal transport, we parameterize the task-space command $\mathbf{u}_{i,t}$ residually:

$$\mathbf{u}_{i,t} = \mathbf{u}_{base} + \mathbf{M} \mathbf{a}_{i,t}, \quad (6)$$

where \mathbf{u}_{base} is produced by a nominal transport controller (e.g., anchor-tracking base motion with a default wrist pose) and \mathbf{M} is a diagonal scaling matrix. The command vector $\mathbf{u}_{i,t}$ governs task-space states:

$$\mathbf{u}_{i,t} = [\mathbf{v}_{base}, H_{com}, \alpha_{ptc}, \mathbf{p}_w]^\top, \quad (7)$$

where $\mathbf{v}_{base} = [v_x, v_y, \dot{\phi}]^\top$ manages locomotion. Wrist positions are modulated as $\mathbf{p}_{w,t} = \bar{\mathbf{p}}_w + \Delta \mathbf{p}_{i,t}$ to manage physical coupling. This structure enables the MARL layer to focus on fine-grained tactical adjustments (e.g., vertical synchronization and compliance), while the WBC layer ensures kinematic/dynamic feasibility and contact stability.

3) *Task-centric reward and heterogeneous learning*: The shared team reward R_t prioritizes strategic progress while enforcing physical safety constraints:

$$R_t = \underbrace{\alpha \cdot \Delta d_{traj}}_{\text{Step-wise progress}} - \underbrace{\beta \sum_{j=1}^4 |z_j - \bar{z}|}_{\text{Tilt penalty}} - \underbrace{\gamma \cdot \mathbb{I}_{drop}}_{\text{Drop penalty}}. \quad (8)$$

Here, Δd_{traj} is the signed displacement toward the current anchor \mathbf{w}_k . Progress is gated by a path-deviation threshold

¹If the object pose is represented in SE(3), $\mathbf{p}_{obj,t}$ denotes its planar position component.

δ to keep the object within a functional corridor. This formulation supports both collaborative carrying and pushing: in carrying, the tilt penalty minimizes z -axis deviations of the object’s corners z_j to maintain level transport; in pushing, these terms vanish when height/tilt are not defined, without biasing the policy. The drop indicator \mathbb{I}_{drop} is a terminal signal triggered by end-effector decoupling or the object falling below a height threshold.

To accommodate agent heterogeneity, we employ independent policies with centralized training and decentralized execution (CTDE). Each agent $i \in \mathcal{N}$ updates its policy π_{θ_i} using a centralized advantage estimate \hat{A}_{tot} :

$$L(\theta_i) = \mathbb{E}_{\tilde{\mathbf{o}}_i, \mathbf{a}} \left[\min \left(r_i(\theta_i) \hat{A}_{tot}, \text{clip}(r_i(\theta_i), 1 - \epsilon, 1 + \epsilon) \hat{A}_{tot} \right) \right] \quad (9)$$

where $r_i(\theta_i)$ is the probability ratio. A joint-action critic $V_\omega(s_t, \mathbf{a}_t)$ with $\mathbf{a}_t = (\mathbf{a}_{i,t}, \mathbf{a}_{-i,t})$ minimizes the temporal-difference (TD) error:

$$\min_{\omega} \left\| V_\omega(s_t, \mathbf{a}_t) - \left(R_t + \gamma V_\omega(s_{t+1}, \mathbf{a}_{t+1}) \right) \right\|^2, \quad (10)$$

which helps stabilize training under non-stationarity by explicitly conditioning value estimates on the joint action.

D. Analysis on the Proposed Architecture

We analyze the proposed methodology from two aspects: (i) mitigation of interaction-induced non-stationarity and (ii) robustness through temporal and functional decomposition.

Proposition 1. In a cooperative Markov game with decentralized policies, a critic that marginalizes over partner actions induces additional non-stationarity in value targets as partner policies evolve. Conditioning the critic on joint actions during centralized training reduces this target drift.

Proof. Consider a decentralized critic

$$Q^{\text{marg}}(s, a_i) = \mathbb{E}_{a_{-i} \sim \pi_{-i}} [Q(s, a_i, a_{-i})].$$

For a fixed joint-action value function $Q(s, a_i, a_{-i})$, changes in π_{-i} during learning alter the marginal distribution over a_{-i} , thereby shifting the induced value target $Q^{\text{marg}}(s, a_i)$. This produces drifting advantage estimates even when $Q(s, a_i, a_{-i})$ itself is held fixed. Under centralized training with a joint-action critic $Q(s, a_i, a_{-i})$, value estimates explicitly condition on realized partner actions, removing the additional target drift introduced by marginalization over a changing partner distribution. Although overall learning dynamics remain non-stationary due to evolving joint policies and state distributions, conditioning on joint actions reduces this specific source of target variation, thereby lowering gradient variance and empirically stabilizing learning. \square

Proposition 2. The decomposition $\mathcal{F} = \mathcal{F}_{WBC} \circ \mathcal{F}_{MARL} \circ \mathcal{F}_{COG}$ separates high-frequency physical stabilization from low-frequency task reasoning.

Proof. Assume the whole-body control layer \mathcal{F}_{WBC} operates at a higher rate f_{high} than the MARL layer rate f_{low} , with $f_{\text{high}} \gg f_{\text{low}}$, and achieves bounded tracking error with respect to task-space references within each MARL update interval. Under this two-timescale separation, the MARL layer \mathcal{F}_{MARL} evolves over a reduced task manifold

defined by anchor tracking, while fast physical perturbations are regulated locally by \mathcal{F}_{WBC} . Perturbations arising from embodiment mismatch or out-of-distribution partner behavior are thus first compensated at the control layer and appear to the higher layers as bounded disturbances rather than amplified deviations. This temporal and functional separation limits cross-layer error coupling and improves robustness under heterogeneous interaction. \square

TABLE I: MARL observation and action space specification.

Component	Dim	Description / Formulation
<i>Observation Space</i> ($\mathbf{o} \in \mathbb{R}^{210}$)		
Global guidance	10	Waypoints along VLM-path
Self state	13	XY pos/vel, yaw, CoM, torso, wrist
Partner state	13	Pose, velocity, and torso pitch
Object geometry	18	4 Corners XYZ, CoM pos/vel
Contact/proximity	40	Binary contact + 36-ray LiDAR
Temporal buffer	116	Snapshots of previous 2 frames
<i>Action Space</i> ($\mathbf{a} \in \mathbb{R}^{11}$)		
Locomotion	3	Absolute $[v_x, v_y, \omega_{yaw}]$
Postural	2	Absolute $H_{\text{CoM}}, \alpha_{\text{torso}}$
Wrist control	6	Relative 3D offsets ($\Delta \mathbf{p}$) per arm

TABLE II: Optimization and topology hyperparameters.

Parameter	Value	Parameter	Value
Learning rate	1.0×10^{-4}	Hidden layers	[256, 256, 128]
Epochs	10	Activation	ReLU
Minibatch	16	Initialization	Orthogonal
Entropy coeff.	0.01	Optimizer	Adam
Discount (γ)	0.99	Weight decay	1.0×10^{-4}
GAE (λ)	0.95	Grad clipping	10.0
Clipping (ϵ)	0.2	LR Schedule	Cosine
Value loss coeff.	0.5	Total steps	2.0×10^9

IV. EXPERIMENTS AND RESULTS

A. Experimental Setup

1) *Nine-scenario collaboration matrix:* We evaluate the proposed cognitive-to-physical hierarchy across a 3×3 grid of embodied coordination challenges, categorized by their distinct kinodynamic and strategic requirements:

- Orientation-sensitive pushing (OSP): evaluates precision in directional transport through S_{11} (alignment), S_{12} (turnaround), and S_{13} (corner entry), requiring precise yaw alignment under external human force.
- Spatially-confined transport (SCT): focuses on synchronized velocity through S_{21} (narrow gate), S_{22} (s-shaped path), and S_{23} (U-shaped path).
- Super-long object handling (SLH): tests complex coordination via S_{31} (facing mode), S_{32} (lateral shuffle), and S_{33} (pivoting), emphasizing the stabilization of payloads.

TABLE III: Global performance matrix: evaluating architectural compatibility across 9 scenarios. The architecture synergy index reflects the mean success rate (SR). The gain Δ highlights the framework’s ability to stabilize heterogeneous solvers compared to the robot-script baseline (calculated as relative improvement).

Category	Scenario	Robot-script	HAPPO	HATRPO	PCGrad	Arch. gain Δ
OSP	S_{11} : Alignment	65.4 ± 7.2	83.6 ± 5.3	87.9 ± 4.5	87.7 ± 3.8	+32.1%
	S_{12} : Turnaround	60.1 ± 8.5	77.6 ± 6.3	81.5 ± 5.5	83.6 ± 4.8	+34.6%
	S_{13} : Corner entry	58.2 ± 9.1	72.7 ± 7.0	75.3 ± 6.0	77.8 ± 5.3	+29.3%
SCT	S_{21} : Narrow gate	59.2 ± 9.0	80.1 ± 4.8	83.4 ± 4.3	88.6 ± 3.5	+42.0%
	S_{22} : S-shaped path	57.5 ± 8.8	76.3 ± 5.8	82.1 ± 5.0	80.6 ± 4.5	+38.6%
	S_{23} : U-shaped path	55.6 ± 9.5	75.7 ± 6.5	79.2 ± 5.3	81.3 ± 4.8	+41.6%
SLH	S_{31} : Facing mode	52.8 ± 8.1	79.3 ± 5.0	84.4 ± 1.6	83.2 ± 3.5	+55.9%
	S_{32} : Lateral shuffle	50.4 ± 7.5	73.7 ± 6.8	75.9 ± 5.8	77.3 ± 5.0	+50.1%
	S_{33} : Pivoting	49.6 ± 8.3	74.9 ± 6.0	77.5 ± 5.3	78.6 ± 4.5	+55.2%
Overall architecture synergy index		56.5%	80.6%	83.0%	83.2%	+45.6%

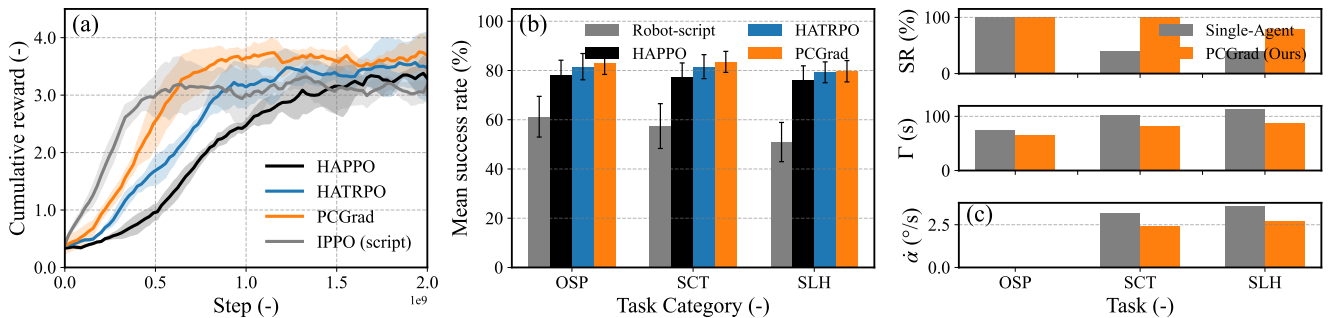


Fig. 4: (a) Episode return during training for the scripted IPPO and the three MARL solvers (HAPPO, HATRPO, PCGrad) over 2.0×10^9 steps. (b) Mean success rate (SR), by task category (OSP, SCT, SLH), comparing the robot-script baseline with the same MARL methods. (c) Real-world deployment: success rate, completion time Γ (s), and mean object tilt rate $\dot{\alpha}$ ($^\circ/s$) for the single-agent baseline versus the MARL candidate.

2) *Simulation and physical platform*: Training is conducted within the Isaac Lab framework [29], utilizing a task-centric Markov potential game formulation. To bridge the sim-to-real gap, physical experiments are executed on a Unitree G1 humanoid robot cooperating with a human partner, with a motion-capture (MoCap) system providing state feedback.

3) *Observation and action spaces*: To facilitate long-horizon coordination without recurrent overhead, we employ a dual-snapshot temporal encoding and a delta-over-base action mechanism. As summarized in Table I, the tactical agent processes a 210-dimensional egocentric observation vector \mathbf{o}_i . The policy outputs an 11-dimensional command vector at 2 Hz, where end-effector control is formulated as spatial offsets ($\Delta \mathbf{p}$) superimposed on task-specific base poses to isolate interaction-driven residuals.

The MARL policy is optimized using the Adam optimizer with the detailed configuration in Table II. We utilize a cosine annealing schedule for the learning rate and orthogonal initialization for all neural network layers to ensure training stability across 2.0×10^9 total action steps.

TABLE IV: Ablation on S_{33} task. No strategic: without VLM anchor generation; No tactical: without MARL coordination buffer; Full hierarchy: the proposed three-layer framework.

Metric	No cognition	No skill	Full hierarchy
VLM strategy	×	✓	✓
MARL skill	✓	×	✓
WBC executive	✓	✓	✓
Success rate	Fails	Fails	78.6%
Efficiency (Γ)	Fails	Fails	81.2 s

B. Architectural Compatibility and Global Performance

We validate the framework’s versatility by integrating three heterogeneous MARL paradigms—HAPPO [30], HATRPO [31], and PCGrad [32]—within the tactical layer. As evidenced in Table III, our hierarchy functions as an algorithm-agnostic HRC architecture, offering seamless plug-and-play compatibility with diverse MARL optimization schemes.

Figure 4 summarizes the main empirical results. Panel (a) reports the episode return (cumulative reward) over 2.0×10^9

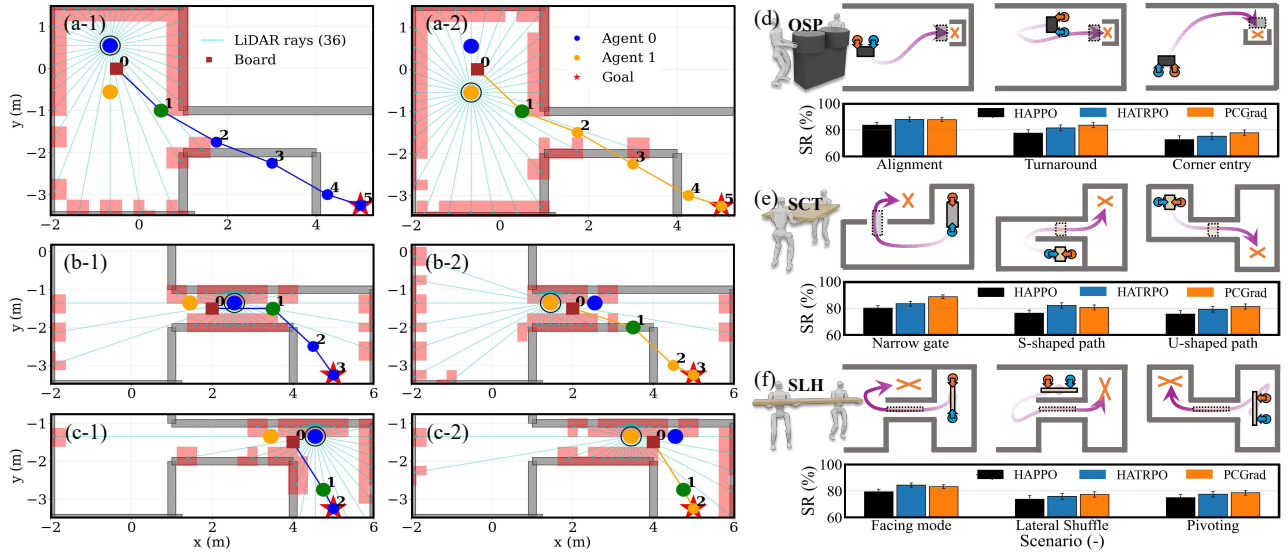


Fig. 5: Visualization of VLM cognitive reasoning and benchmarking results. (a)-(c) illustrate the spatial reasoning in the S_{33} task, where -1 and -2 refer to the views of different agents. The cyan lines represent synthetic LiDAR rays, and the green dot denotes the anchor guiding the skill layer. (d)-(f) present the task and success rate (SR) statistics for all scenarios.

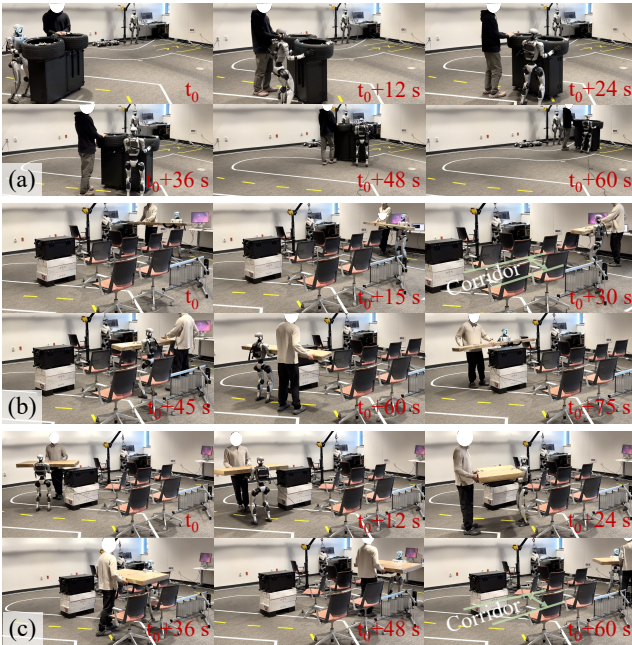


Fig. 6: Time-series visualization of human-robot collaboration: the snapshots capture the agents’ ability to execute smooth turns, and navigate through gate and corridor.

environment steps for the scripted baseline (IPPO) and the three MARL solvers (HAPPO, HATRPO, PCGrad) integrated in our hierarchy. All learning curves are aligned to a common initial value and scale; the MARL policies consistently outperform the scripted baseline and converge to higher returns. Panel (b) shows the mean success rate Φ by task category (OSP, SCT, SLH), averaged over the nine scenarios of Table III. The MARL-based tactical layer again improves

over the robot-script baseline across categories, with the overall architecture synergy index exceeding 80% for all three algorithms. Panel (c) turns to real-world deployment on the Unitree G1 humanoid. Compared with a single-agent RL baseline under the same hierarchical structure, the proposed PCGrad variant achieves higher success rates Φ , shorter task completion times Γ , and lower object tilt rates $\hat{\alpha}$ on the SCT and SLH tasks, illustrating the benefit of multi-agent coordination in the tactical layer.

TABLE V: Real-world quantitative metrics (mean over 5 trials). Single-agent RL and PCGrad both utilize the proposed hierarchy. SR: success rate; $\hat{\alpha}$: mean object tilt rate; Γ : task completion time.

Task	Single-Agent Baseline			PCGrad (MARL)		
	SR	$\hat{\alpha}$ ($^{\circ}/s$)	Γ (s)	SR	$\hat{\alpha}$ ($^{\circ}/s$)	Γ (s)
OSP	100%	–	74.2	100%	–	65.2
SCT	40%	3.2	101.6	100%	2.4	81.5
SLH	40%	3.6	113.6	80%	2.7	86.9

The task-level robustness and cognitive depth of our hierarchy are visualized in Fig. 5. By processing multi-view observations into synthetic LiDAR representations (cyan rays), the VLMs successfully resolve a collision-free CoM trajectory for each agent (visualized as blue and orange paths). The generation of discrete navigation anchors demonstrates how the open-vocabulary reasoning is grounded into executable spatial goals for the downstream MARL policy. Panels (a)-(c) illustrate the internal mechanism of the semantic cognitive layer during a complex pivoting maneuver. More importantly, panels (d)-(f) validate the high success rates across diverse collaborative challenges.

To isolate the contribution of each hierarchical layer, we compare three configurations on task S_{33} . Table IV provides the quantitative breakdown, confirming that the full three-layer hierarchy is essential for effective coordination. The qualitative performance of the proposed hierarchy during physical deployment is visualized in Fig. 6.

The time-series snapshots across various tasks (a-c) demonstrate the seamless coordination between the G1 humanoid robot and its human partner. As the human initiates movement or direction changes, the robot’s tactical layer—guided by the VLM’s strategic anchors—internalizes the partner’s intent to maintain stable object leveling and contact. These sequences highlight the framework’s resilience in long-horizon transport and its ability to bridge the cognitive-to-physical gap in unstructured, real-world-like settings. The physical deployment on the Unitree G1 emphasizes coordination resilience. Table V compares the performance when the tactical layer is hosted by a Single-Agent baseline versus the proposed multi-agent PCGrad variant, both integrated with our architecture.

V. CONCLUSION

This work introduces cognition-to-control (C2C), a three-layer hierarchy that makes the deliberation-to-control pathway explicit for human–robot collaboration. By decomposing the system into a VLM-based grounding layer, a deliberative skill/coordination layer, and a whole-body control layer, C2C translates high-level intent into contact-stable whole-body motion while adapting to a human partner under contact, feasibility, and safety constraints. The grounding layer maintains persistent scene referents and infers embodiment-aware affordances/constraints; the skill layer converts this task structure into long-horizon, role-free coordination via MARL; and the control layer executes the resulting commands at low latency while enforcing kinodynamic feasibility.

- We formulate HRC as a task-centric Markov potential game where leader-follower behaviors arise implicitly as stable coordination patterns under a shared task potential, without explicit role encoding. Our MARL layer internalizes partner dynamics and mitigates interaction bias without explicit role assignment, ensuring decentralized coordination remains globally consistent.
- The concurrent MARL paradigm enables mutual adaptation from a tabula rasa state, forcing agents to explore diverse interaction configurations. This process serves as an inherent data augmentation mechanism that densifies the interaction space and significantly enhances the policy’s feasibility during deployment.
- Real-world experiments demonstrate that our framework achieves a 45.6% performance gain over robot-script baselines in complex tasks, showing superior resilience and lower object tilt rates. More broadly, C2C suggests that stable human–robot collaboration can be achieved by explicitly separating semantic reasoning from embodiment-aware tactical coordination.

- [1] O. Khatib, K. Yokoi, O. Brock, K. Chang, and A. Casal, “Robots in human environments: Basic autonomous capabilities,” *The International Journal of Robotics Research*, vol. 18, no. 7, pp. 684–696, 1999.
- [2] H. S. Koppula and A. Saxena, “Anticipating human activities using object affordances for reactive robotic response,” *IEEE transactions on pattern analysis and machine intelligence*, vol. 38, no. 1, pp. 14–29, 2015.
- [3] G. Li, B. He, R. Gomez, and K. Nakamura, “Interactive reinforcement learning from demonstration and human evaluative feedback,” in *2018 27th IEEE International Symposium on Robot and Human Interactive Communication (RO-MAN)*. IEEE, 2018, pp. 1156–1162.
- [4] U. E. Ogenyi, J. Liu, C. Yang, Z. Ju, and H. Liu, “Physical human–robot collaboration: Robotic systems, learning methods, collaborative strategies, sensors, and actuators,” *IEEE transactions on cybernetics*, vol. 51, no. 4, pp. 1888–1901, 2019.
- [5] D. Strouse, M. Kleiman-Weiner, J. Joshmer, and J. B. Tenenbaum, “Collaborating with humans without human data,” in *Advances in Neural Information Processing Systems (NeurIPS)*, vol. 34, 2021.
- [6] M. Carroll, R. Shah, M. K. Ho, T. Griffiths, S. Seshia, P. Abbeel, and A. Dragan, “On the utility of learning about humans for human-ai coordination,” *Advances in neural information processing systems*, vol. 32, 2019.
- [7] H. Zhang, N. Lei, S. E. Li, J. Zhang, and Z. Wang, “Multi-scale reinforcement learning of dynamic energy controller for connected electrified vehicles,” *IEEE Transactions on Intelligent Transportation Systems*, vol. 26, no. 12, pp. 22 607–22 619, 2025.
- [8] D. Balduzzi, S. Racaniere, J. Martens, J. Foerster, K. Tuyls, and T. Graepel, “The mechanics of n-player differentiable games,” in *Proceedings of the 35th International Conference on Machine Learning*, 2018, pp. 354–363.
- [9] G. Papoudakis, F. Christianos, L. Schäfer, and S. V. Albrecht, “Benchmarking multi-agent deep reinforcement learning algorithms in cooperative tasks,” *arXiv preprint arXiv:2006.07869*, 2020.
- [10] S. Gronauer and K. Diepold, “Multi-agent deep reinforcement learning: a survey,” *Artificial Intelligence Review*, vol. 55, no. 2, pp. 895–943, 2022.
- [11] B. Baker, I. Kanitscheider, T. Markov, Y. Wu, G. Powell, B. McGrew, and I. Mordatch, “Emergent tool use from multi-agent autocurricula,” in *International conference on learning representations*, 2019.
- [12] M. Murooka, T. Hoshi, K. Fukumitsu, S. Masuda, M. Hamze, T. Sasaki, M. Morisawa, and E. Yoshida, “Tact: Humanoid whole-body contact manipulation through deep imitation learning with tactile modality,” *IEEE Robotics and Automation Letters*, 2025.
- [13] S. Izquierdo-Badiola, G. Canal, C. Rizzo, and G. Alenyà, “Plancollabnl: Leveraging large language models for adaptive plan generation in human-robot collaboration,” in *2024 IEEE International Conference on Robotics and Automation (ICRA)*. IEEE, 2024, pp. 17 344–17 350.
- [14] A. S. Chen, A. M. Lessing, A. Tang, G. Chada, L. Smith, S. Levine, and C. Finn, “Commonsense reasoning for legged robot adaptation with vision-language models,” pp. 12 826–12 833, 2025.
- [15] W. Huang, F. Xia, T. Xiao, H. Chan, J. Liang, P. Florence, A. Zeng, J. Tompson, I. Mordatch, Y. Chebotar *et al.*, “Inner monologue: Embodied reasoning through planning with language models,” 2022.
- [16] A. Ajay, Y. Du, A. Gupta, J. Tenenbaum, T. Jaakkola, and P. Agrawal, “Is conditional generative modeling all you need for decision-making?” *arXiv preprint arXiv:2211.15657*, 2022.
- [17] J. Li, X. Cheng, T. Huang, S. Yang, R. Qiu, and X. Wang, “Amo: Adaptive motion optimization for hyper-dexterous humanoid whole-body control,” in *Robotics: Science and Systems*, 2025.
- [18] M. J. Kim, K. Pertsch, S. Karamcheti, T. Xiao, A. Balakrishna, S. Nair, R. Rafailov, E. Foster, G. Lam, P. Sanketi *et al.*, “Openvla: An open-source vision-language-action model,” *arXiv preprint arXiv:2406.09246*, 2024.
- [19] A. Rioux and W. Suleiman, “Humanoid navigation and heavy load transportation in a cluttered environment,” pp. 2180–2186, 2015.
- [20] M. Ahn, A. Brohan, N. Brown, Y. Chebotar, O. Cortes, B. David, C. Finn, C. Fu, K. Gopalakrishnan, K. Hausman *et al.*, “Do as i can, not as i say: Grounding language in robotic affordances,” 2022.
- [21] N. Hogan, “Impedance control: An approach to manipulation,” pp. 304–313, 1984.
- [22] D. Hadfield-Menell, S. J. Russell, P. Abbeel, and A. Dragan, “Cooperative inverse reinforcement learning,” *Advances in neural information processing systems*, vol. 29, 2016.

- [23] J. Lo, G. Huang, and D. Metaxas, "Human motion planning based on recursive dynamics and optimal control techniques," *Multibody System Dynamics*, vol. 8, no. 4, pp. 433–458, 2002.
- [24] J. Lekeufack, A. N. Angelopoulos, A. Bajcsy, M. I. Jordan, and J. Malik, "Conformal decision theory: Safe autonomous decisions from imperfect predictions," in *2024 IEEE International Conference on Robotics and Automation (ICRA)*. IEEE, 2024, pp. 11 668–11 675.
- [25] A. Oroojlooy and D. Hajinezhad, "A review of cooperative multi-agent deep reinforcement learning," *Applied Intelligence*, vol. 53, no. 11, pp. 13 677–13 722, 2023.
- [26] R. Lowe, Y. I. Wu, A. Tamar, J. Harb, O. Pieter Abbeel, and I. Mordatch, "Multi-agent actor-critic for mixed cooperative-competitive environments," *Advances in neural information processing systems*, vol. 30, 2017.
- [27] H. Kang, X. Chang, J. Mišić, V. B. Mišić, J. Fan, and Y. Liu, "Cooperative uav resource allocation and task offloading in hierarchical aerial computing systems: A mapo-based approach," *IEEE Internet of Things Journal*, vol. 10, no. 12, pp. 10 497–10 509, 2023.
- [28] Q. Liu, X. Zhang, M. Tan, S. Ma, J. Ding, and Y. Li, "Mash: Cooperative-heterogeneous multi-agent reinforcement learning for single humanoid robot locomotion," *arXiv preprint arXiv:2508.10423*, 2025.
- [29] M. Mittal, C. Yu, Q. Yu, J. Liu, N. Rudin, D. Hoeller, J. L. Yuan, R. Singh, Y. Guo, H. Mazhar *et al.*, "Orbit: A unified simulation framework for interactive robot learning environments," *IEEE Robotics and Automation Letters*, vol. 8, no. 6, pp. 3740–3747, 2023.
- [30] Y. Zhong, J. G. Kuba, X. Feng, S. Hu, J. Ji, and Y. Yang, "Heterogeneous-agent reinforcement learning," *Journal of Machine Learning Research*, vol. 25, no. 32, pp. 1–67, 2024.
- [31] J. G. Kuba, R. Chen, M. Wen, Y. Wen, F. Sun, J. Wang, and Y. Yang, "Trust region policy optimisation in multi-agent reinforcement learning," *arXiv preprint arXiv:2109.11251*, 2021.
- [32] T. Yu, S. Kumar, A. Gupta, S. Levine, K. Hausman, and C. Finn, "Gradient surgery for multi-task learning," *Advances in neural information processing systems*, vol. 33, pp. 5824–5836, 2020.